Published in final edited form as:
Mol Imaging Biol. 2011 December ; 13(6): 1224–1233. doi:10.1007/s11307-010-0458-y.

MicroPET Imaging of Integrin $\alpha_v\beta_3$ Expressing Tumors Using ^{89}Zr-RGD Peptides

Orit Jacobson[1], **Lei Zhu**[1,2], **Gang Niu**[1], **Ido D. Weiss**[3], **Lawrence P. Szajek**[4], **Ying Ma**[1], **Xilin Sun**[1], **Yongjun Yan**[1], **Dale O. Kiesewetter**[1], **Shuang Liu**[5], and **Xiaoyuan Chen**[1]

[1]Laboratory of Molecular Imaging and Nanomedicine (LOMIN), National Institute of Biomedical Imaging and Bioengineering (NIBIB), National Institutes of Health (NIH), Bldg. 31, Room 1C22, Bethesda, MD, 20892, USA

[2]Key Laboratory for Molecular Enzymology and Enzyme Engineering of the Ministry of Education, Jilin University, Jilin, 130000, China

[3]Laboratory of Molecular Immunology, National Institute of Allergy and Infectious Diseases (NIAID), National Institutes of Health (NIH), Bethesda, MD, USA

[4]Department of Positron Emission Tomography, Warren Grant Magnuson Clinical Center, National Institutes of Health, Bethesda, MD, USA

[5]School of Health Sciences, Purdue University, West Lafayette, IN, USA

Abstract

Purpose—The dimeric transmembrane integrin, $\alpha_v\beta_3$, is a well-investigated target by different imaging modalities through suitably labeled arginine–glycine–aspartic acid (RGD) containing peptides. In this study, we labeled four cyclic RGD peptides with or without PEG functional groups: c(RGDfK) (denoted as FK), PEG_3-c(RGDfK) (denoted as FK-PEG_3), E[c(RGDfK)]$_2$ (denoted as [FK]$_2$), and PEG_4-E[PEG_4-c(RGDfK)]$_2$ (denoted as [FK]$_2$-3PEG_4), with ^{89}Zr ($t_{1/2}$=78.4 h), using the chelator desferrioxamine-p-SCN (Df) for imaging tumor integrin $\alpha_v\beta_3$.

Methods—The Df conjugated RGD peptides were subjected to integrin $\alpha_v\beta_3$ binding assay *in vitro* using MDA-MB-435 breast cancer cells. The ^{89}Zr-labeled RGD peptides were then subjected to small animal positron emission tomography (PET) and direct tissue sampling biodistribution studies in an orthotopic MDA-MB-435 breast cancer xenograft model.

Results—All four tracers, ^{89}Zr-Df-FK, ^{89}Zr-Df-FK-PEG_3, ^{89}Zr-Df-[FK]$_2$, and ^{89}Zr-Df-[FK]$_2$-3PEG_4, were labeled in high radiochemical yield (89±4%) and high specific activity (4.07–6 MBq/μg). Competitive binding assay with ^{125}I-echistatin showed that conjugation of the RGD peptides to the Df chelator did not have significant impact on their integrin $\alpha_v\beta_3$ binding affinity and the dimeric peptides were shown to be more potent than the monomers. In agreement with binding results, tumor uptake of ^{89}Zr-Df-[FK]$_2$ and ^{89}Zr-Df-[FK]$_2$-3PEG_4 was significantly higher (4.32±1.73%ID/g and 4.72±0.66%ID/g, respectively, at 2 h post-injection) than the monomers ^{89}Zr-Df-FK and ^{89}Zr-Df-FK-PEG_3 (1.97±0.38%ID/g and 1.57±0.49%ID/g, respectively, at 2 h post-injection). Out of the four labeled peptides, ^{89}Zr-Df-[FK]$_2$-3PEG_4 gave the highest tumor-to-background ratio (18.21±2.52 at 2 h post-injection and 19.69±3.99 at 4 h post-injection), with the lowest uptake in metabolic organs. Analysis of late time points

Correspondence to: Xiaoyuan Chen; shawn.chen@nih.gov.

Conflict of Interest Statement. Authors declare that they have no conflict of interest.

biodistribution data revealed that the uptake in the tumor was decreased, along with increase in the bone, which implies decomplexation of ^{89}Zr-Df.

Conclusion—Efficient radiolabeling of peptides with an appropriate chelator such as Df-RGD with ^{89}Zr was observed. The ^{89}Zr radiolabeled peptides provided high-quality and high-resolution microPET images in xenograft models. ^{89}Zr-Df-$[FK]_2$-$3PEG_4$ demonstrated the highest tumor-to-background ratio of the compounds tested. Preparation of ^{89}Zr peptides to take advantage of the longer half-life is unwarranted due to the relatively rapid clearance from the tumor region of peptide tracers prepared for this study and the increased uptake in the bone of transchelated ^{89}Zr with time (2.0±0.36%ID/g, 24 h post-injection).

Keywords

^{89}Zr—zirconium; RGD peptides; Integrin $\alpha_v\beta_3$; PET

Introduction

Angiogenesis (new vessel formation) is a crucial process for tumor growth and metastasis [1–8]. In order to induce angiogenesis, angiogenic factors are released by the tumor to activate endothelial cells in established blood vessels and induce endothelial proliferation and migration.

Integrins are a family of heterodimeric transmembrane glycoproteins which play an essential role in the regulation of cellular adhesion, migration, proliferation, survival, signal transduction, and differentiation [7–9]. One member of this receptors class is the dimeric transmembrane integrin, $\alpha_v\beta_3$, which is expressed at low levels on epithelial cells and mature endothelial cells. Upon activation of endothelial cells, $\alpha_v\beta_3$ is upregulated on the cell membrane. In addition, several tumors including osteosarcomas, neuroblastomas, glioblastomas, melanomas, lung carcinomas, and breast cancers were shown to express this integrin [1,10–13]. Hence, integrin $\alpha_v\beta_3$ expression can be targeted for imaging tumor growth, invasion, and metastasis, and for treatment of the rapidly growing and metastatic tumors [1,14–16].

Integrin $\alpha_v\beta_3$ interacts with extracellular matrix proteins (e.g., vitronectin, tenascin, fibronectin, and collagen) through their exposed arginine–glycine–aspartic acid (RGD) amino acid moieties and it regulates the migration of endothelial cells through the extracellular matrix during vessel formation [17–20]. A number of cyclic RGD peptide moieties have been investigated as imaging probes for monitoring integrin $\alpha_v\beta_3$ expression level in tumors, using different molecular imaging modalities such as positron emission tomography (PET), single photon emission computed tomography, optical imaging, magnetic resonance imaging, and ultrasound [6,8,14,21–33]. For radionuclide imaging of integrin $\alpha_v\beta_3$ expression *in vivo*, tumor-targeting efficacy and *in vivo* kinetic profiles are highly related to the receptor-binding affinity and specificity, hydrophilicity, molecular size, and overall molecular charge of the resulting radiotracers [13].

Here we report on the evaluation of four different cyclic RGD peptides (Fig. 1) labeled with a relatively long-lived PET isotope, zirconuim-89 (^{89}Zr, $t_{1/2}$=78.4 h, β^+=22.7%, maximum β^+ energy=0.897 MeV, electron capture=76.6%), to visualize integrin $\alpha_v\beta_3$ expression *in vivo*.

The long half-life of ^{89}Zr along with its other physical properties make it a favorable isotope for labeling antibodies which have slow pharmacokinetics *in vivo*, and it allows tracking and quantification for longer periods. We hypothesized that labeling RGD peptides with ^{89}Zr may give high-resolution PET images at delayed time points. In this study, we evaluated the

differences between the four labeled RGD peptides in terms of binding affinity and tumor-targeting efficacy *in vivo*. Determining tumor integrin $\alpha_v\beta_3$ expression by using ^{89}Zr-RGD peptides and PET scan could be useful in predicting tumor behavior and responses to antiangiogenic therapies, including therapies targeting integrin $\alpha_v\beta_3$. This could lead to more effective "personalized" cancer treatments.

Materials and Methods

General

Desferrioxamine-p-SCN (Df) was purchased from Macrocyclics (Dallas, TX, USA). All other solvents and chemicals were purchased from Sigma-Aldrich (St. Louis, MO, USA).

C_{18} cartridges (Waters Corporation, Milford, MA, USA) were each activated with 5 mL of EtOH and 10 mL of water. Radio-TLC was performed on an AR-2000 Bioscan scanner (Washington DC, USA), using silica gel plates (LK6DF, 60Å, 200 mm, Whatman) and citric buffer (pH=4.9) as a developing solvent. c(RGDfk) (denoted as FK), E[c(RGDfk)$_2$] (denoted as [FK]$_2$), and E[c (RGDfk)$_2$]-3PEG$_4$ (denoted as [FK]$_2$-3PEG$_4$) were purchased from Peptides International (Louisville, KY, USA).

Synthesis of NH_2-Mini-PEG-c(RGDfk) (PEG_3-c(RGDfk))

PEG$_3$-c(RGDfk) (denoted as FK-PEG$_3$) was prepared according to a known procedure [34]. Briefly, to a solution of Boc-11-amino-3,6,9-trioxaundecanoic acid (Boc-NH-mini-PEG-COOH, 0.51 mg, 1.66 mmol) and 0.26 mL *N*,*N*-diisopropylethylamine in acetonitrile (ACN) was added *O*-(*N*-succinimidyl)-1,1,3,3-tetramethyl-uronium tetrafluoroborate (0.34 mg, 1.15 mmol). The reaction mixture was stirred at room temperature for 0.5 h and then added to c(RGDfk) (28 mg, 46 μmol) in *N*,*N*′-dimethylformamide. The reaction was stirred at room temperature for another 2 h and the desired product, Boc-NH-mini-PEG-c(RGDfk), was isolated by semipreparative high-performance liquid chromatography (HPLC). The collected fractions were combined and lyophilized to give a fluffy white powder (60% yield). The Boc group was readily removed by treating Boc-NH-mini-PEG-c(RGDfk) with anhydrous trifluoroacetic acid (TFA) for 5 min at room temperature. The crude product was purified on a reversed-phase HPLC system using a Higgins preparative C_{18} column (5 μm, 20×250 mm). The flow was set at 12 mL/min using a gradient system, starting from 95% of solvent A (0.1% TFA in water) and 5% of solvent B (0.1% TFA in ACN) and increasing to 35% solvent A and 65% solvent B at 35 min. The desired peptide had a retention time of 13.8 min. The collected fractions were combined and lyophilized to afford FK-PEG$_3$ as a white powder.

Conjugation of the Peptides with Df

The conjugation procedure of Df with RGD peptide moieties was conducted by dissolving the peptide (1–2 mg) in 0.2–0.3 mL dimethylsulfoxide (DMSO). Then, 1.2 eq. of Df in 0.1 mL of DMSO were added, followed by addition of 5 eq. of diisopropylethylamine. The reaction was mixed at room temperature for 4–5 h. Purification of the conjugated peptides was conducted on a reversed-phase HPLC system using a Higgins preparative C_{18} column (5 μm, 20×250 mm). The flow was set at 12 mL/min using a gradient system, starting from 95% of solvent A (0.1% TFA in water) and 5% of solvent B (0.1% TFA in ACN) and increasing to 35% solvent A and 65% solvent B at 35 min. The retention times were as follows: Df-FK, 24.8 min; Df-FK-PEG$_3$, 24.1 min; Df-[FK]$_2$, 23.9 min; and Df-[FK]$_2$-3PEG$_4$, 19.8 min. The desired peptide conjugates were collected and the solvent was removed by lyophilization.

Mass Spectrometry Analysis

LC/MS analysis employed a Waters LC–MS system (Waters Corporation) that included an Acquity UPLC system coupled to the Waters Q-Tof Premier high-resolution mass spectrometer. An Acquity BEH Shield RP18 column (150×2.1 mm) was employed for chromatography. Elution was achieved with a binary mixture of two components. Solution A was composed of 2 mM ammonium formate, 0.1% formic acid, and 5% ACN; solution B was composed of 2 mM ammonium formate and 0.1% formic acid in ACN. The elution profile, at 0.35 mL/min, had the following components: initial condition at 100% (v:v) A and 0% B; gradient 0–40% B over 5 min; isocratic elution at 40% B for an additional 5 min; 40–80% B over 2 min; and re-equilibrated with A for an additional 3 min. The retention time for Df-FK and Df-FK-PEG_3 were 5.13 min and 5.09 min, respectively. The retention time for Df-$[FK]_2$ and Df-$[FK]_2$-$3PEG_4$ were 4.65 min and 4.72 min, respectively. The injection volume was 10 μL. The entire column elute was introduced into the Q-Tof mass spectrometer. Ion detection was achieved in ESI mode using a source capillary voltage of 3.5 kV, source temperature of 110°C, desolvation temperature of 200°C, cone gas flow of 50 L/h (N_2), and desolvation gas flow of 700 L/h (N_2). LC–MS confirmed the molecular mass of the conjugated peptides: Df-FK (*m/z*): observed 1,357.57 [$M+H^+$], calculated: 1,356.62; Df-FK-PEG_3: observed 1,545.75 [$M+H^+$], calculated: 1,544.75; Df-$[FK]_2$: observed 1,036.59 [$(M+2H^+)/2$], calculated: 2,071.38; Df-$[FK]_2$-$3PEG_4$, 1,419.35 [$(M+2H^+)/2$] (calculated: 2,841.30).

^{89}Zr Production

Pressed pellets of yttrium metal mesh (200 mg, 4 N purity; American Elements) were irradiated with a proton beam of 15 MeV and a current of 20 μA for 2–4 h on a GE PETtrace cyclotron. The production rate was 1.17±0.05 mCi/μA h (*n*=10). ^{89}Zr was separated as ^{89}Zr-oxalate from the irradiated yttrium mesh using the method of Holland and co-workers [35]. Briefly, to a mini-vial charged with the irradiated metal was carefully added 6 N HCl (4×0.5 mL) and ultra-pure 10 M H_2O_2 (100 μL, Fluka). The resulting solution was warmed to 80°C before dilution with 18 mΩ H_2O (5 mL) and loading onto a pre-washed column of hydroxamate resin (200 mg). The resin was washed with 2 N HCl (4×2.5 mL) followed by 18 mΩ H_2O (4×2.5 mL). ^{89}Zr was eluted with 1.0 M oxalic acid (4×0.5 mL and 2×1.0 mL) in greater than 96% radiochemical yield. The ^{89}Zr-oxalate yield for a 2-h irradiation was 44.2±2.1 mCi (*n*=6) at end of bombardment.

^{89}Zr Radiolabeling

^{89}Zr labeling was done similarly to the known procedure [36]. Briefly, 220 μL of ^{89}Zr-oxalate (1.6–2.2 mCi, 59–81 MBq) was transferred into a glass tube, followed by addition of 100 μL 2 M Na_2CO_3. The reaction was incubated for 2–3 min at room temperature. Thereafter, 0.5 mL of 0.5 M HEPES buffer (pH=7.2) was added to the reaction vial. The pH of the reaction vial was measured to be approximately 7–7.2. Df-RGD conjugate (10–20 μg) (Df-FK, Df-FK-PEG_3, Df-$[FK]_2$, and Df-$[FK]_2$-$3PEG_4$) dissolved in 1–2 μL of DMSO and 0.3 mL of 0.5 M HEPES buffer (pH=7.2) was added to the reaction vial. The reaction was briefly vortexed and incubated at room temperature for 20 min. Complexation of ^{89}Zr and the Df-RGD peptide conjugates were monitored by radio-TLC (R_f [^{89}Zr-Df-RGD]=0–0.05, R_f [^{89}Zr-free]=0.3). For all four Df-RGD conjugates, radio-TLC showed incorporation of greater than 95%. The reaction vial was then diluted with 10 mL of water and loaded onto an activated C_{18} Sep-Pak cartridge. The cartridge was washed with water (10 mL) and the desired labeled peptide (^{89}Zr-Df-FK, ^{89}Zr-Df-FK-PEG_3, ^{89}Zr-Df-$[FK]_2$, and ^{89}Zr-Df-$[FK]_2$-$3PEG_4$) was eluted with 10 mM HCl in ethanol (1 mL) into a glass test tube. The ethanol was evaporated for 2–3 min under astream of argon at 60°C and then reformulated with phosphate-buffered saline (PBS).

MDA-MB-435 Cell Culture

MDA-MB-435 cell line was purchased from American Type Culture Collection and grown in Leibovitz's L-15 medium (Gibco) supplemented with 10% (v/v) fetal bovine serum at 37°C under an atmosphere containing 5% CO_2.

Integrin $\alpha_v\beta_3$ Receptor Competition Cell Binding Assay

Competition cell binding assay was done using integrin $\alpha_v\beta_3$-specific radioligand, ^{125}I-echistatin. MDA-MB-435 cells were grew up to 80% confluence and then scraped off and resuspended with binding buffer [25 mM 2-amino-2-(hydroxymethyl)-1,3-propanediol, hydrochloride (Tris–HCl), pH 7.4, 150 mM NaCl, 1 mM $CaCl_2$, 0.5 mM $MgCl_2$ and 1 mM $MnCl_2$, 0.1% bovine serum albumin (BSA)]. Incubation was conducted in a 96-well plate with each well containing 2×10^5 cells, 0.02 μCi (0.74 kBq) ^{125}I-echistatin (Perkin-Elmer) and 0–5,000 nM of FK, Df-FK, and Df-FK-PEG_3 or 0–500 nM of Df-$[FK]_2$ and Df-$[FK]_2$-$3PEG_4$ in 200 μL for 2 h on a shaker at room temperature. After incubation, cells were washed three times with cold PBS containing 0.1% BSA. Thereafter, the plate was heated to 40°C and dried. The dried filter membranes were punched from the wells, collected in polystyrene culture test tubes (12×75 mm), and counted for cell bound radioactivity (1480 Wizard 3 gamma counter; Perkin-Elmer). The IC_{50} values were calculated by nonlinear regression analysis using the GraphPad Prism fitting program (GraphPad Software, Inc., San Diego, CA, USA). Each data point is a result of the average of duplicate wells.

Tumor Xenograft Model

Athymic nude mice were purchased from Harlan (Frederick, MD, USA) and housed under pathogen-free conditions. All animal studies were conducted in accordance with the principles and procedures outlined in the National Institutes of Health (NIH) Guide for the Care and Use of Animals, and under protocols approved by the NIH Clinical Center Animal Care and Use Committee. The MDA-MB-435 tumor model was generated by orthotopic injection of 5×10^6 cells in the left mammary fat pad of each female athymic nude mouse.

PET Studies

Tumor-bearing mice were anesthetized using isoflurane/O_2 (1.5–2% v/v) and injected with 100 μCi (3.7 MBq) of ^{89}Zr-Df-FK, ^{89}Zr-Df-FK-PEG_3, ^{89}Zr-Df-$[FK]_2$, or ^{89}Zr-Df-$[FK]_2$-$3PEG_4$ in a volume of 150 μL PBS. PET scans were performed using an Inveon DPET scanner (Siemens Medical Solutions) at 0.5, 1, 2, 4, and 24 h post-injection. For blocking experiments, 100 μCi (3.7 MBq) of ^{89}Zr-Df-$[FK]_2$-$3PEG_4$ were co-injected with 300 μg of unlabeled c(RGDfk). Each group contained four to five mice. The images were reconstructed by a three-dimensional ordered subsets expectation maximum (3D-OSEM) algorithm, and no correction was applied for attenuation or scatter. Image analysis was done using ASI Pro VM™ software. The percentage of injected dose per gram (%ID/g) for the various tissues was determined by drawing regions of interest (ROIs) surrounding the entire organ on the coronal images. The radioactivity contained in the ROI divided by the dose administered to the animal gave the %ID and the volume of the ROI was converted to mass assuming a density of 1 for all tissues.

Biodistribution

Each mouse was intravenously injected 100 μCi (3.7 MBq) of ^{89}Zr-Df-FK, ^{89}Zr-Df-FK-PEG_3, ^{89}Zr-Df-$[FK]_2$, or ^{89}Zr-Df-$[FK]_2$-$3PEG_4$ in a volume of 150 μL PBS. At different time points post-injection, blood was drawn from the heart, under anesthesia, and the mice were then sacrificed. Liver, muscle, kidneys, intestine, bone, spleen, pancreas, lung, stomach, heart, and tumor were removed. The organs were wet weighed and assayed for

radioactivity using a gamma counter. For blocking experiment, 300 μg of unlabeled c(RGDfk) were co-injected with the appropriately labeled peptide. Each group contained four to five mice.

Statistical Analysis

Results were expressed as mean and SD. Two-tailed paired and unpaired Student's *t* tests were used to determine differences within groups and between groups, respectively. *P* values <0.05 were considered statistically significant.

Results

Chemistry and Radiochemistry

Conjugation of Df with RGD peptides was done in DMSO in the presence of diisopropylethylamine at room temperature, to give the conjugated peptides in high chemical yield of 80–90%, after HPLC purification. After lyophilization, the conjugated Df-RGD peptides were obtained as fluffy white powders. The Df-RGD conjugates were not completely soluble in water; therefore, a concentrated stock solution (10 mg/mL) of each conjugate was prepared in DMSO. For the radiolabeling, only 10–20 μg of each Df-RGD peptide was diluted with 0.5 M HEPES buffer for each reaction.

^{89}Zr complexation into the desired Df-RGD peptides was very efficient. Following incubation at room temperature for 20 min, almost no free ^{89}Zr was detected by radio-TLC. The overall radiochemical yield for all peptides was 89±4% (not decay-corrected), calculated from the start of synthesis to the reformulation of the labeled peptide with PBS. ^{89}Zr-Df-RGD peptides were achieved with specific activity of 0.11–0.18 mCi/μg (4.07–6.7 MBq/μg).

Competitive Binding Assay with ^{125}I-Echistatin Radioligand

The affinity of Df-FK, Df-FK-PEG_3, Df-$[FK]_2$, and Df-$[FK]_2$-$3PEG_4$ to integrin $\alpha_v\beta_3$ was tested using the human breast carcinoma cell line MDA-MB-435, which is known to express medium level of the integrin [13]. Binding affinities of the Df-RGD conjugates were compared to that of c(RGDfk) (FK) (Fig. 2). The IC_{50}s of Df-RGD monomers Df-FK and Df-FK-PEG_3 were 305 nM and 408 nM, respectively, which is similar to that of FK (350 nM). The Df-RGD dimers (Df-$[FK]_2$ and Df-$[FK]_2$-$3PEG_4$) are more potent than the monomeric counterparts, with IC_{50}s of 78 nM for Df-$[FK]_2$ and 22 nM for Df-$[FK]_2$-$3PEG_4$.

MicroPET Imaging Studies in Tumor-Bearing Mice

The tumor-targeting efficacy of ^{89}Zr-Df-FK, ^{89}Zr-Df-FK-PEG_3, ^{89}Zr-Df-$[FK]_2$, and ^{89}Zr-Df-$[FK]_2$-$3PEG_4$ in MDA-MB-435 tumor mice was evaluated by static microPET scans. The %ID/g was calculated for the tumor, blood, muscle, liver, bone, and kidneys (Figs. 3 and 4). The tumor uptakes of the monomeric RGD peptides (^{89}Zr-Df-FK and ^{89}Zr-Df-FK-PEG_3) at all time points were lower than those of the dimeric RGD peptides ^{89}Zr-Df-$[FK]_2$ and ^{89}Zr-Df-$[FK]_2$-$3PEG_4$ (Figs. 3 and 4). ^{89}Zr-Df-FK had tumor uptake of 2.3±0.4%ID/g at 1 h post-injection, which remained constant at 2 h (2.0±0.38%ID/g), but was decreased by half at 13 h post-injection (Fig. 3a). ^{89}Zr-Df-FK-PEG_3 had slightly lower tumor uptake (1.63±0.35%ID/g at 1 h and 1.57±0.49%ID/g at 2 h post-injection) than ^{89}Zr-Df-FK (Fig. 3b). Similar to ^{89}Zr-Df-FK, the uptake of ^{89}Zr-Df-FK-PEG_3 in the tumor at 13 h post-injection was also decreased by half (Fig. 3b). The tumor-to-blood ratios of ^{89}Zr-Df-FK and ^{89}Zr-Df-FK-PEG_3 at 1 h post-injection were 4.46±0.80 and 3.37±0.87, respectively (Table 1). These ratios were increased to 8.71±1.81 for ^{89}Zr-Df-FK and 6.33±1.27 for ^{89}Zr-Df-FK-PEG_3 at 2 h post-injection, probably due to the clearance of the labeled peptide from the blood. The highest uptake of ^{89}Zr-Df-FK and ^{89}Zr-Df-FK-PEG_3 was observed in the

liver, which remained high at 13 h post-injection (approximately 15%ID/g, Fig. 3). Comparison of the kidney uptake between ^{89}Zr-Df-FK and ^{89}Zr-Df-FK-PEG$_3$ showed that ^{89}Zr-Df-FK had higher renal uptake at all time points (Fig. 3).

^{89}Zr-Df-[FK]$_2$ had high tumor uptake at 0.5 h post-injection (4.51±1.46%ID/g), which remained high at 4 h post-injection (4.44±1.03%ID/g), with a high tumor-to-blood ratio of 16.58±1.54 at 4 h time point (Table 1). Nevertheless, at 24 h post-injection, the uptake in the tumor was decreased to 2.69±0.43%ID/g (Fig. 4a). ^{89}Zr-Df-[FK]$_2$ also had high uptake in the liver at all time points (approximately 12–17% ID/g, Fig. 4a). The kidney uptake of ^{89}Zr-Df-[FK]$_2$ was high up to 4 h post-injection (10.6±3.49%ID/g), which was decreased by half at 24 h post-injection (Fig. 4a). ^{89}Zr-Df-[FK]$_2$-3PEG$_4$ showed high and persistent tumor uptake (3.98±0.50%ID/g at 0.5 h to 4.47±0.81%ID/g at 4 h, Fig. 4b). At 4 h post-injection, a high tumor-to-blood ratio was attained for ^{89}Zr-Df-[FK]$_2$-3PEG$_4$ (19.69±3.99, Table 1). However, the tumor uptake of ^{89}Zr-Df-[FK]$_2$-3PEG$_4$ was significantly decreased at 24 h to 2.2±0.26%ID/g (Fig. 4b), which resulted in a reduced tumor-to-blood ratio (10.82±1.31, Table 1). The uptake of ^{89}Zr-Df-[FK]$_2$-3PEG$_4$ in the liver and kidneys was significantly lower than those of the other three ^{89}Zr-Df-RGD peptides (Fig. 4b).

Representative coronal images of ^{89}Zr-Df-[FK]$_2$-3PEG$_4$ at different time points post-injection are shown in Fig. 5. MDA-MB-435 tumors were clearly visualized with good tumor-to-background contrast at 0.5, 1, 2, and 4 h post-injection (Fig. 5). At 24 h, the uptake in the tumor was decreased, while uptake in the joints and bones was elevated. Therefore, at 24 h post-injection, visualization by PET of the tumor was limited by the low tumor-to-background ratio (Fig. 5).

In order to determine the specific binding to integrin $\alpha_v\beta_3$*in vivo*, tumor-bearing mice were co-injected with ^{89}Zr-Df-[FK]$_2$-3PEG$_4$ and an excess of unlabeled c(RGDfk) (FK) (300 μg per mouse). The uptake in the tumor was decreased by approximately 90% (0.39±0.01%ID/g), confirming the specific binding to integrin $\alpha_v\beta_3$ (Fig. 5). The uptake in the liver and kidneys was elevated due to the blocking in the tumor (Fig. 5).

Biodistribution Studies

Biodistribution of ^{89}Zr-Df-FK and ^{89}Zr-Df-FK-PEG$_3$ in tumor-bearing mice were done at 24 h post-injection of the labeled peptides (Table 2). Both peptides had high uptake in the liver (22.25±4.79%ID/g for ^{89}Zr-Df-FK and 17.20±7.64%ID/g for ^{89}Zr-Df-FK-PEG$_3$, respectively). High uptake was also found in the kidneys (10.72±1.04%ID/g for ^{89}Zr-Df-FK and 5.65±1.10%ID/g for ^{89}Zr-Df-FK-PEG$_3$). ^{89}Zr-Df-FK and ^{89}Zr-Df-FK-PEG$_3$ uptake in the intestine was low (1.14±0.20%ID/g and 0.71±0.07%ID/g, respectively, Table 1). Surprisingly, both peptides had high uptake in the spleen (7.19±2.13%ID/g for ^{89}Zr-Df-FK and 8.94±5.89%ID/g for ^{89}Zr-Df-FK-PEG$_3$). In comparison with the PET data at earlier time points (1 and 2 h post-injection, Fig. 3), higher uptake was observed in the bone (1.71±0.59%ID/g for ^{89}Zr-Df-FK and 1.14±0.30%ID/g for ^{89}Zr-Df-FK-PEG$_3$, Table 2), suggesting the release of ^{89}Zr from its chelator, Df. The tumor uptake in the tumor at 24 h post-injection was low for both RGD monomers; 1.01±0.08% ID/g and 0.73±0.07%ID/g for ^{89}Zr-Df-FK and ^{89}Zr-Df-FKPEG$_3$, respectively.

Biodistribution of ^{89}Zr-Df-[FK]$_2$ in tumor-bearing mice was determined at 4 h post-injection (Table 3). The results are in good agreement with the PET image quantification (Fig. 4a). Higher uptake of ^{89}Zr-Df-[FK]$_2$ was observed in the liver (17.46±1.85%ID/g) and the kidneys (21.11±3.41% ID/g, Table 3). The uptake in the tumor was high (4.04±0.73%ID/g).

For ^{89}Zr-Df-[FK]$_2$-3PEG$_4$, biodistribution in tumor-bearing mice was measured at 4 h post-injection, with and without adding the unlabeled RGD peptide. The uptake in the liver,

for ^{89}Zr-Df-[FK]$_2$-3PEG$_4$, was significantly lower (6.8±0.73%ID/g, Fig. 6) than the other three labeled peptides, probably due to higher hydrophilicity of this peptide. The uptake in the tumor was fairly high (3.94±0.38%ID/g), and this uptake was successfully blocked (reduced to 0.4±0.01%ID/g) when ^{89}Zr-Df-[FK]$_2$-3PEG$_4$ was co-injected with an excess of unlabeled c(RGDfk) (Fig. 6). The blocking studies resulted in significant elevation of the uptake in the liver (increased from 6.81±0.71%ID/g to 18.79±2.21%ID/g), kidneys (increased from 5.93±0.93%ID/g to 16.70±2.74%ID/g), and the spleen (increased from 3.76±0.31%ID/g to 9.50±1.30%ID/g, Fig. 6).

Discussion

RGD peptides labeled with various radionuclides were previously investigated for both tumor-targeted imaging and therapy [7,16,30,37–39]. However, no RGD peptide was previously labeled with ^{89}Zr. ^{89}Zr-labeled antibodies showed promising results for immunoPET imaging [40–43]. ^{89}Zr has a positron emission decay of 902 KeV, which provides microPET resolution similar to ^{18}F and ^{11}C [41]. The long half-life (78.4 h) of ^{89}Zr allows imaging mice for a long period of time post-injection of the tracer.

In this study, we evaluated the potential of ^{89}Zr as a labeling radionuclide for imaging integrin $\alpha_v\beta_3$ expressing tumors. Two RGD peptide monomers (c(RGDfk) (FK) and c(RGDfk)-PEG$_3$ (FK-PEG$_3$)) and two RGD peptide dimers (E[c(RGDfk)$_2$ ([FK]$_2$) and E[c(RGDfk)$_2$-3PEG$_4$ ([FK]$_2$-3PEG$_4$)) were coupled to the chelator, desferrioxamine-p-SCN (Df), for the complexation with ^{89}Zr (Fig. 1).

The labeling with ^{89}Zr was very straightforward. The complexation of ^{89}Zr into the chelator was efficient and all the peptides achieved high radiochemical yield (89±4%) and high specific activity of 4.07–6.7 MBq/μg. Conjugation of the RGD peptides to Df chelator did not have a significant impact on their integrin $\alpha_v\beta_3$ binding affinity and *in vitro* competitive binding assay against ^{125}I-echistatin showed that the rank order of integrin $\alpha_v\beta_3$ binding affinities of Df-RGD peptides were Df-[FK]$_2$-3PEG$_4$>Df-[FK]$_2$>Df-FK>Df-FK-PEG$_3$≈ FK (Fig. 2).

Comparison of PET scans and biodistribution data between the four ^{89}Zr-Df-RGD peptides showed that they all cleared rapidly from the blood (Figs. 3 and 4). Nevertheless, comparison of ^{89}Zr-RGD peptides to RGD peptides labeled with other PET isotopes as reported literature [6–8,13,33,34,44] demonstrate that ^{89}Zr-RGD peptides had higher blood uptake at later time points. For example, ^{89}Zr-Df-[FK]$_2$-3PEG$_4$ had approximately 0.67%ID/g in the blood, 4 h post-injection. Shi et al. reported a value of 0.15%ID/g at 4 h post-injection, when the peptide was coupled to DOTA and labeled with ^{64}Cu [44]. This phenomenon might be due to the conjugation to Df, which have reduced clearance rate from the blood.

^{89}Zr-Df-FK and ^{89}Zr-Df-FK-PEG$_3$ had high uptake in metabolic organs, such as liver and kidneys, at all time points (Fig. 3 and Table 2). ^{89}Zr-Df-FK-PEG$_3$ had faster clearance through the kidneys than ^{89}Zr-Df-FK (Fig. 3). These differences in the pharmacokinetics were attributed to the addition of PEG functional group, which increases the hydrophilicity of the peptide and therefore accelerates the clearance of the peptide through the kidneys. ^{89}Zr-Df-FK had slightly higher, but not significant, tumor uptake than ^{89}Zr-Df-FK-PEG$_3$ at 1 and 2 h post-injection (Fig. 3). However, tumor-to-blood ratios were similar for both peptides (8.71±1.81 for ^{89}Zr-Df-FK and 6.33±1.27 for ^{89}Zr-Df-FK-PEG$_3$ at 2 h post-injection). The ability to image later time points because of the longer half-life of ^{89}Zr was of little advantage as the tumor uptake was decreased at later time points and excretion tissues increased. Even the slower clearance of the dimeric ligands could be observed by 4 h.

Out of the four peptides, the dimeric peptides gave better tumor uptake and tumor-to-blood ratio (Fig. 4 and Table 1) than the monomeric analogs. This may be explained by the bivalent binding of the dimer to integrins on the cell surface, which significantly reduces the dissociation of the tracer from its target [44]. Between the two dimers, ^{89}Zr-Df-[FK]$_2$-3PEG$_4$ had slightly better imaging figure of merit, probably due to the longer spacer connecting the two RGD moieties, that confers less limitation on the distance between integrins on the cell surface [44]. The presence of three short PEG groups is also expected to have an effect on the tumor targeting and *in vivo* kinetics. Accordingly, ^{89}Zr-Df-[FK]$_2$-3PEG$_4$ had the best overall tumor-to-background contrast and serves as an appropriate integrin imaging agent. Blocking studies by co-injection of ^{89}Zr-Df-[FK]$_2$-3PEG$_4$ and unlabeled c(RGDfk) showed a significant decrease in the tumor uptake, suggesting a specific binding of this tracer to integrin $\alpha_v\beta_3$. In this same experiment, blocking was detected in other organs, such as stomach, pancreas, intestine, heart, and muscle, which suggests that the binding of ^{89}Zr-Df-[FK]$_2$-3PEG$_4$ to these organs is partially integrin $\alpha_v\beta_3$ mediated.

Biodistribution studies for all four peptides showed unexpectedly high uptake in the spleen which does not express high level of integrin $\alpha_v\beta_3$. This phenomenon has not been reported in other radiolabeled RGD peptides. Moreover, in blocking studies the accumulation in the spleen, liver, and kidneys was increased (Fig. 6), suggesting that this accumulation is not integrin specific but can be related to ^{89}Zr. Another hypothesis is that increasing amounts of unlabeled peptide (≥300 μg) which had to be cleared could have been redirected to clearance routes other than the kidneys, such as uptake by hepatocytes and macrophages.

An elevated uptake was also detected in the bones and joints 24 h post-injection (Figs. 4 and 5, Table 2), which implies the decomplexation of ^{89}Zr from the Df chelator [43]. Although ^{89}Zr has favorable positron emission decay compared to other radiometals, elevated uptake in the bone and the decreased uptake in the tumor over time result in reduced tumor visualization by microPET scans.

Other chelators for zirconium such as desferrioxamine B (DFO), derivatives of DFO using amino reactive linkers and thiol reactive linkers [41,43], and diethylenetriaminepentaacetic acid (DTPA) [45] have been evaluated; however, decomplexation of the zirconium and uptake in the bone was evident in all of them at 24 h or longer time points post-injection. The need for a more stable chelator that does not undergo decomplexation *in vivo* has not been met.

Conclusions

^{89}Zr-Df-FK, ^{89}Zr-Df-FK-PEG$_3$, ^{89}Zr-Df-[FK]$_2$, and ^{89}Zr-Df-[FK]$_2$-3PEG$_4$ were shown to bind specifically to integrin $\alpha_v\beta_3$ expressing MDA-MB-435 cells *in vitro* and MDA-MB-435 orthotopic xenografts *in vivo*, with ^{89}Zr-Df-[FK]$_2$-3PEG$_4$ giving the most promising results. However, at later time points, decomplexation of ^{89}Zr and its accumulation in the bone, along with a decrease in the tumor uptake due to fast clearance of peptides, suggest that labeling RGD peptides with long half-life isotope such as ^{89}Zr is not favorable. Further optimization of the chelator structures for more stable ^{89}Zr complexation is needed.

Acknowledgments

This research was supported by the Intramural Research Program (IRP) of the National Institute of Biomedical Imaging and Bioengineering (NIBIB).

References

1. Liu S. Radiolabeled cyclic RGD peptides as integrin αvβ3-targeted radiotracers: maximizing binding affinity via bivalency. Bioconjug Chem. 2009; 20:2199–2213. [PubMed: 19719118]
2. Carmeliet P, Jain RK. Angiogenesis in cancer and other diseases. Nature. 2000; 407:249–257. [PubMed: 11001068]
3. Carmeliet P. Mechanisms of angiogenesis and arteriogenesis. Nat Med. 2000; 6:389–395. [PubMed: 10742145]
4. Sengupta S, Chattopadhyay N, Mitra A, Ray S, Dasgupta S, Chatterjee A. Role of αvβ3 integrin receptors in breast tumor. J Exp Clin Cancer Res. 2001; 20:585–560. [PubMed: 11876555]
5. Wang L, Shi J, Kim YS, Zhai S, Jia B, Zhao H, et al. Improving tumor-targeting capability and pharmacokinetics of ^{99m}Tc-labeled cyclic RGD dimers with PEG_4 linkers. Mol Pharm. 2009; 6:231–245. [PubMed: 19067525]
6. Chen X, Park R, Hou Y, Khankaldyyan V, Gonzales-Gomez I, Tohme M, et al. MicroPET imaging of brain tumor angiogenesis with ^{18}F-labeled PEGylated RGD peptide. Eur J Nucl Med Mol Imaging. 2004; 31:1081–1089. [PubMed: 15118844]
7. Chen X, Liu S, Hou Y, Tohme M, Park R, Bading JR, et al. MicroPET imaging of breast cancer αv-integrin expression with ^{64}Cu-labeled dimeric RGD peptides. Mol Imaging Biol. 2004; 6:350–359. [PubMed: 15380745]
8. Chen X, Tohme M, Park R, Hou Y, Bading JR, Conti PS. MicroPET imaging of αvβ3-integrin expression with ^{18}F-labeled dimeric RGD peptide. Mol Imaging. 2004; 3:96–104. [PubMed: 15296674]
9. Dijkgraaf I, Beer AJ, Wester HJ. Application of RGD-containing peptides as imaging probes for αvβ3 expression. Front Biosci. 2009; 14:887–899. [PubMed: 19273106]
10. Bello L, Francolini M, Marthyn P, Zhang J, Carroll RS, Nikas DC, et al. αvβ3 and αvβ5 integrin expression in glioma periphery. Neurosurgery. 2001; 49:380–389. discussion 90. [PubMed: 11504114]
11. Felding-Habermann B, Mueller BM, Romerdahl CA, Cheresh DA. Involvement of integrin αv gene expression in human melanoma tumorigenicity. J Clin Invest. 1992; 89:2018–2022. [PubMed: 1376331]
12. Robinson SD, Reynolds LE, Wyder L, Hicklin DJ, Hodivala-Dilke KM. β3-integrin regulates vascular endothelial growth factor-A-dependent permeability. Arterioscler Thromb Vasc Biol. 2004; 24:2108–2114. [PubMed: 15345507]
13. Zhang X, Xiong Z, Wu Y, Cai W, Tseng JR, Gambhir SS, et al. Quantitative PET imaging of tumor integrin αvβ3 expression with ^{18}F-FRGD2. J Nucl Med. 2006; 47:113–121. [PubMed: 16391195]
14. Chen X. Multimodality imaging of tumor integrin αvβ3 expression. Mini Rev Med Chem. 2006; 6:227–234. [PubMed: 16472190]
15. Cai W, Niu G, Chen X. Imaging of integrins as biomarkers for tumor angiogenesis. Curr Pharm Des. 2008; 14:2943–2973. [PubMed: 18991712]
16. Liu S. Radiolabeled multimeric cyclic RGD peptides as integrin αvβ3 targeted radiotracers for tumor imaging. Mol Pharm. 2006; 3:472–487. [PubMed: 17009846]
17. Bogler O, Mikkelsen T. Angiogenesis in glioma: molecular mechanisms and roadblocks to translation. Cancer J. 2003; 9:205–213. [PubMed: 12952305]
18. Hwang R, Varner J. The role of integrins in tumor angiogenesis. Hematol Oncol Clin North Am. 2004; 18:991–1006. vii. [PubMed: 15474331]
19. Brooks PC, Montgomery AM, Rosenfeld M, Reisfeld RA, Hu T, Klier G, et al. Integrin αvβ3 antagonists promote tumor regression by inducing apoptosis of angiogenic blood vessels. Cell. 1994; 79:1157–1164. [PubMed: 7528107]
20. Brooks PC, Clark RA, Cheresh DA. Requirement of vascular integrin αvβ3 for angiogenesis. Science. 1994; 264:569–571. [PubMed: 7512751]
21. Dayton PA, Pearson D, Clark J, Simon S, Schumann PA, Zutshi R, et al. Ultrasonic analysis of peptide- and antibody-targeted micro-bubble contrast agents for molecular imaging of αvβ3-expressing cells. Mol Imaging. 2004; 3:125–134. [PubMed: 15296677]

22. Ellegala DB, Leong-Poi H, Carpenter JE, Klibanov AL, Kaul S, Shaffrey ME, et al. Imaging tumor angiogenesis with contrast ultrasound and microbubbles targeted to αvβ3. Circulation. 2003; 108:336–341. [PubMed: 12835208]
23. Leong-Poi H, Christiansen J, Klibanov AL, Kaul S, Lindner JR. Noninvasive assessment of angiogenesis by ultrasound and micro-bubbles targeted to αv-integrins. Circulation. 2003; 107:455–460. [PubMed: 12551871]
24. Sipkins DA, Cheresh DA, Kazemi MR, Nevin LM, Bednarski MD, Li KC. Detection of tumor angiogenesis *in vivo* by αvβ3-targeted magnetic resonance imaging. Nat Med. 1998; 4:623–626. [PubMed: 9585240]
25. Chen X, Conti PS, Moats RA. *In vivo* near-infrared fluorescence imaging of integrin αvβ3 in brain tumor xenografts. Cancer Res. 2004; 64:8009–8014. [PubMed: 15520209]
26. Chen X, Park R, Shahinian AH, Tohme M, Khankaldyyan V, Bozorgzadeh MH, et al. ^{18}F-labeled RGD peptide: initial evaluation for imaging brain tumor angiogenesis. Nucl Med Biol. 2004; 31:179–189. [PubMed: 15013483]
27. Chen X, Park R, Tohme M, Shahinian AH, Bading JR, Conti PS. MicroPET and autoradiographic imaging of breast cancer αv-integrin expression using ^{18}F- and ^{64}Cu-labeled RGD peptide. Bioconjug Chem. 2004; 15:41–49. [PubMed: 14733582]
28. Chen X, Park R, Shahinian AH, Bading JR, Conti PS. Pharmacokinetics and tumor retention of ^{125}I-labeled RGD peptide are improved by PEGylation. Nucl Med Biol. 2004; 31:11–19. [PubMed: 14741566]
29. Chen X, Hou Y, Tohme M, Park R, Khankaldyyan V, Gonzales-Gomez I, et al. Pegylated Arg-Gly-Asp peptide: ^{64}Cu labeling and PET imaging of brain tumor αvβ3-integrin expression. J Nucl Med. 2004; 45:1776–1783. [PubMed: 15471848]
30. Haubner R, Wester HJ, Weber WA, Mang C, Ziegler SI, Goodman SL, et al. Noninvasive imaging of αvβ3 integrin expression using ^{18}F-labeled RGD-containing glycopeptide and positron emission tomography. Cancer Res. 2001; 61:1781–1785. [PubMed: 11280722]
31. Haubner R, Bruchertseifer F, Bock M, Kessler H, Schwaiger M, Wester HJ. Synthesis and biological evaluation of a ^{99m}Tc-labelled cyclic RGD peptide for imaging the αvβ3 expression. Nuklearmedizin. 2004; 43:26–32. [PubMed: 14978538]
32. Haubner R, Kuhnast B, Mang C, Weber WA, Kessler H, Wester HJ, et al. [^{18}F]Galacto-RGD: synthesis, radiolabeling, metabolic stability, and radiation dose estimates. Bioconjug Chem. 2004; 15:61–69. [PubMed: 14733584]
33. Li ZB, Chen K, Chen X. ^{68}Ga-labeled multimeric RGD peptides for microPET imaging of integrin αvβ3 expression. Eur J Nucl Med Mol Imaging. 2008; 35:1100–1108. [PubMed: 18204838]
34. Wu Z, Li ZB, Chen K, Cai W, He L, Chin FT, et al. microPET of tumor integrin αvβ3 expression using ^{18}F-labeled PEGylated tetrameric RGD peptide (^{18}F-FPRGD4). J Nucl Med. 2007; 48:1536–1544. [PubMed: 17704249]
35. Holland JP, Sheh Y, Lewis JS. Standardized methods for the production of high specific-activity zirconium-89. Nucl Med Biol. 2009; 36:729–739. [PubMed: 19720285]
36. Vosjan MJ, Perk LR, Visser GW, Budde M, Jurek P, Kiefer GE, et al. Conjugation and radiolabeling of monoclonal antibodies with zirconium-89 for PET imaging using the bifunctional chelate p-isothiocyanatobenzyl-desferrioxamine. Nat Protoc. 2010; 5:739–743. [PubMed: 20360768]
37. Wu Y, Zhang X, Xiong Z, Cheng Z, Fisher DR, Liu S, et al. microPET imaging of glioma integrin αvβ3 expression using ^{64}Cu-labeled tetrameric RGD peptide. J Nucl Med. 2005; 46:1707–1718. [PubMed: 16204722]
38. Janssen M, Oyen WJ, Massuger LF, Frielink C, Dijkgraaf I, Edwards DS, et al. Comparison of a monomeric and dimeric radiolabeled RGD-peptide for tumor targeting. Cancer Biother Radiopharm. 2002; 17:641–646. [PubMed: 12537667]
39. Haubner R, Wester HJ, Reuning U, Senekowitsch-Schmidtke R, Diefenbach B, Kessler H, et al. Radiolabeled αvβ3 integrin antagonists: a new class of tracers for tumor targeting. J Nucl Med. 1999; 40:1061–1071. [PubMed: 10452325]

40. Dijkers EC, Oude Munnink TH, Kosterink JG, Brouwers AH, Jager PL, de Jong JR, et al. Biodistribution of ^{89}Zr-trastuzumab and PET imaging of HER2-positive lesions in patients with metastatic breast cancer. Clin Pharmacol Ther. 2010; 87:586–592. [PubMed: 20357763]

41. Tinianow JN, Gill HS, Ogasawara A, Flores JE, Vanderbilt AN, Luis E, et al. Site-specifically ^{89}Zr-labeled monoclonal antibodies for ImmunoPET. Nucl Med Biol. 2010; 37:289–297. [PubMed: 20346868]

42. Hoeben BA, Kaanders JH, Franssen GM, Troost EG, Rijken PF, Oosterwijk E, et al. PET of hypoxia with ^{89}Zr-labeled cG250-F(ab′)2 in head and neck tumors. J Nucl Med. 2010; 51:1076–1083. [PubMed: 20554724]

43. Holland JP, Divilov V, Bander NH, Smith-Jones PM, Larson SM, Lewis JS. ^{89}Zr-DFO-J591 for immunoPET of prostate-specific membrane antigen expression *in vivo*. J Nucl Med. 2010; 51:1293–1300. [PubMed: 20660376]

44. Shi J, Kim YS, Zhai S, Liu Z, Chen X, Liu S. Improving tumor uptake and pharmacokinetics of ^{64}Cu-labeled cyclic RGD peptide dimers with Gly_3 and PEG_4 linkers. Bioconjug Chem. 2009; 20:750–759. [PubMed: 19320477]

45. Meijs WE, Herscheid JDM, Haisma H, Pinedo HM. Evaluation of desferal as a bifunctional chelating agent for labeling antibodies with Zr-89. Appl Radiat Isot. 1992; 43:1443–1447.

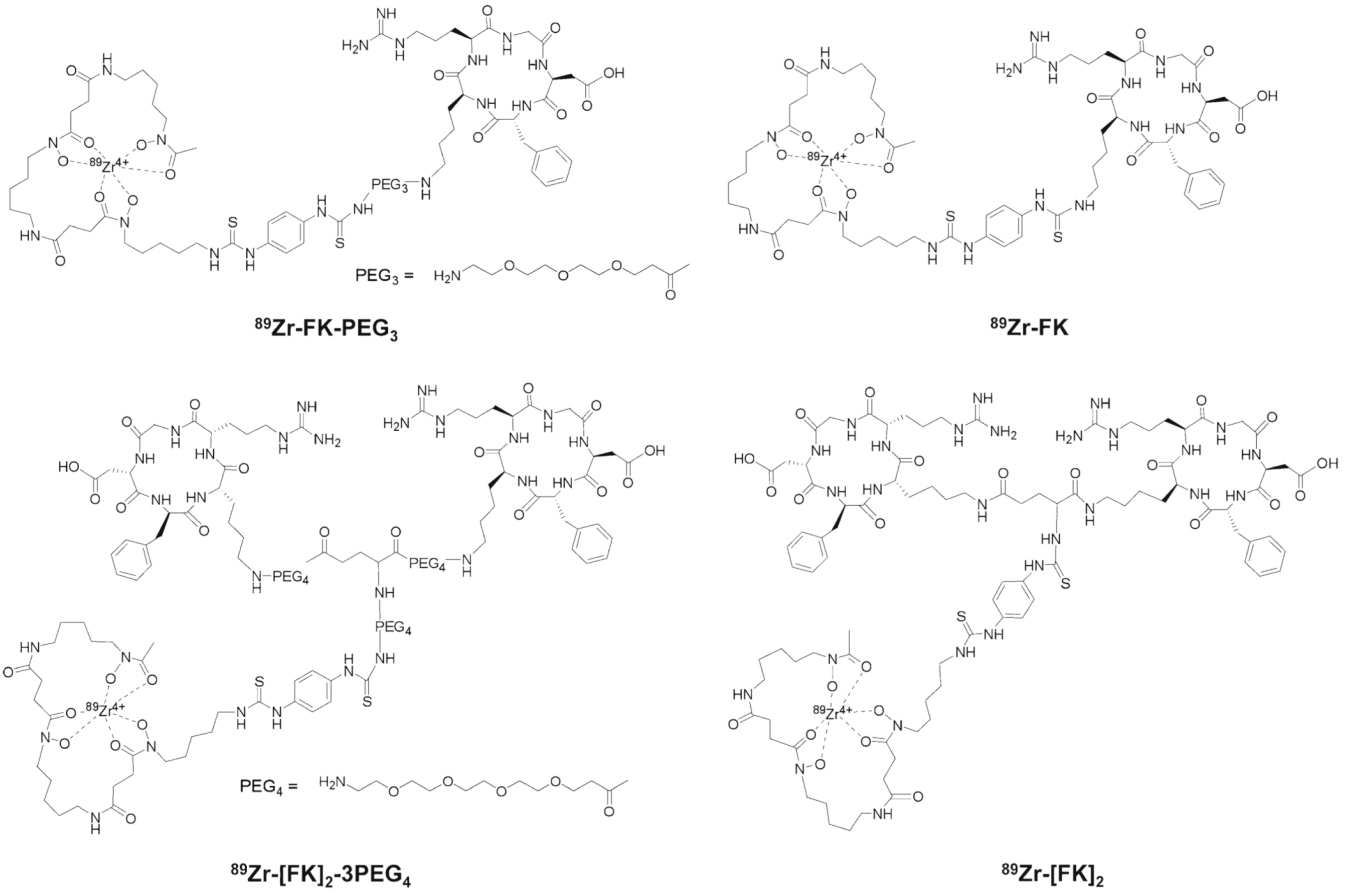

Fig. 1.
Chemical structures of ^{89}Zr-Df-RGD peptide conjugates.

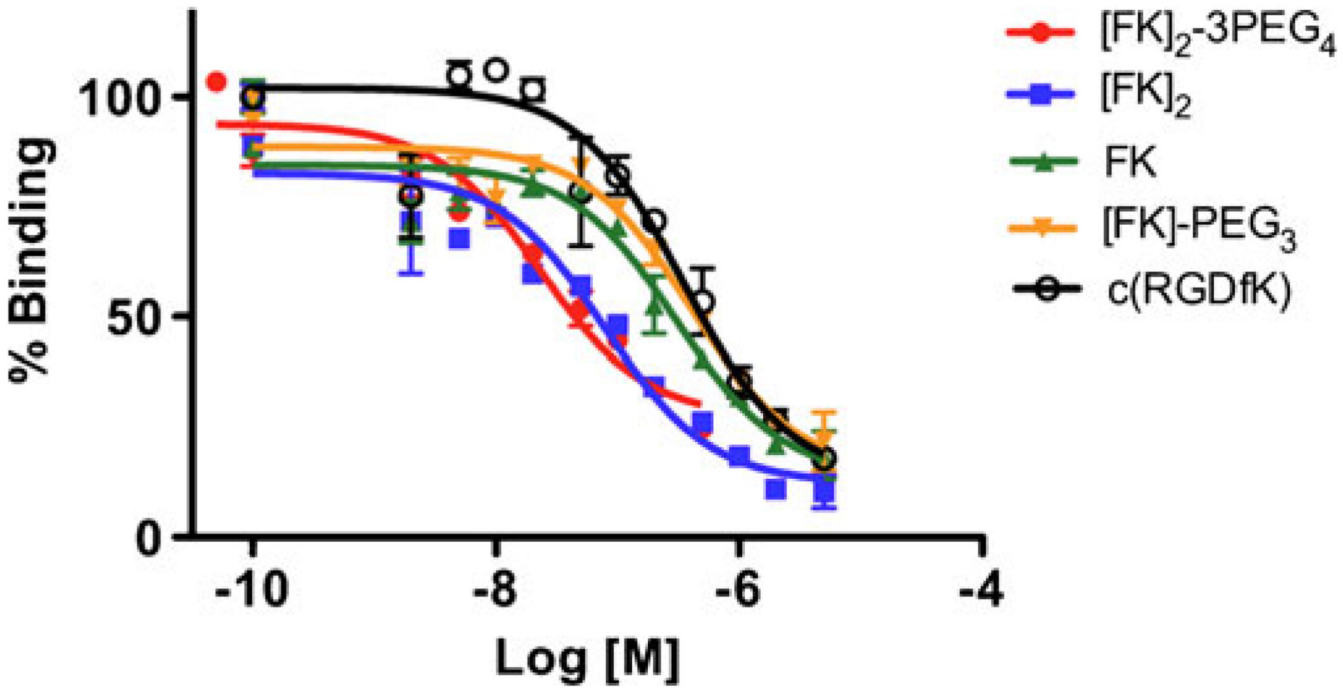

Fig. 2.

Inhibition of ^{125}I-echistatin binding to $\alpha_v\beta_3$ integrin in MDA-MB-435 cells by Df-$[FK]_2$-$3PEG_4$, Df-$[FK]_2$, Df-FK, Df-FK-PEG_3, and c(RGDfk).

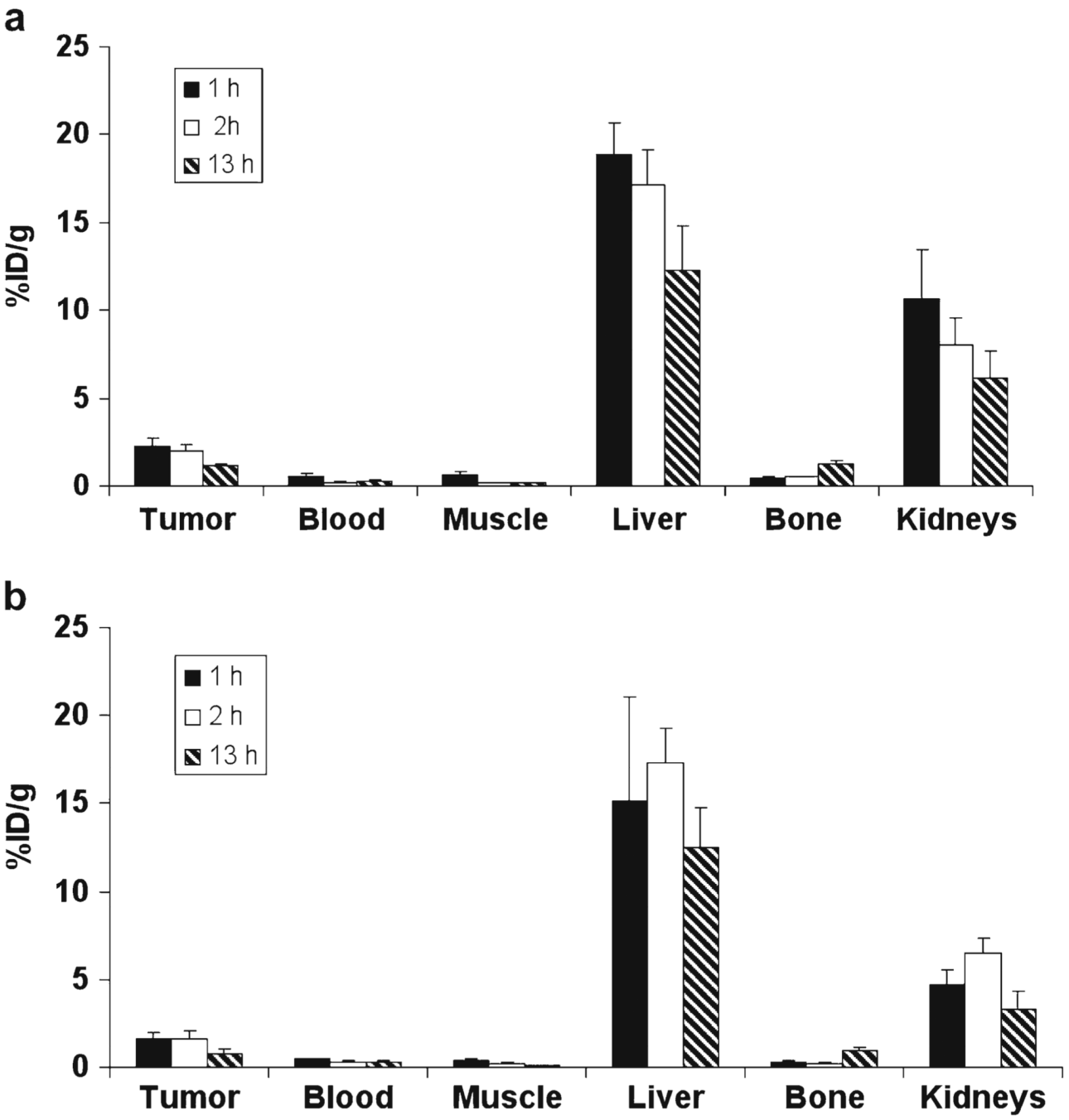

Fig. 3.

Uptake of ^{89}Zr-Df-FK (**a**) and ^{89}Zr-Df-FK-PEG$_3$ (**b**) in MDA-MB-435 tumor-bearing mice at 1, 2, and 13 h post-injection. Results are calculated from PET scans and are shown as averages of 4–5 mice±SD.

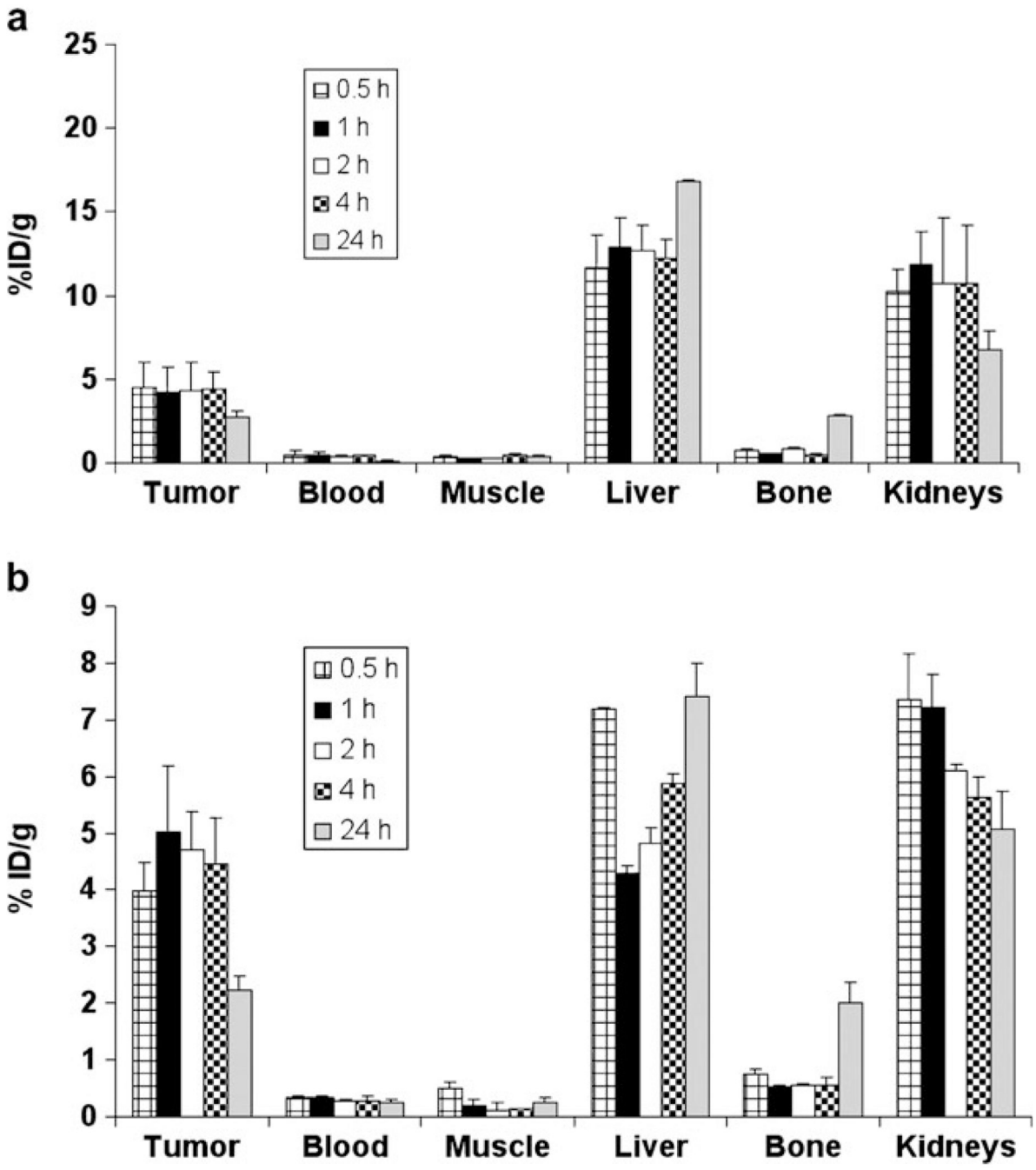

Fig. 4.

Uptake of ^{89}Zr-Df-[FK]$_2$ (**a**) and ^{89}Zr-Df-[FK]$_2$-3PEG$_4$ (**b**) in MDA-MB-435 tumor-bearing mice at 0.5, 1, 2, 4, and 24 h post-injection. Results are calculated from PET scans and are shown as averages of 4–5 mice±SD.

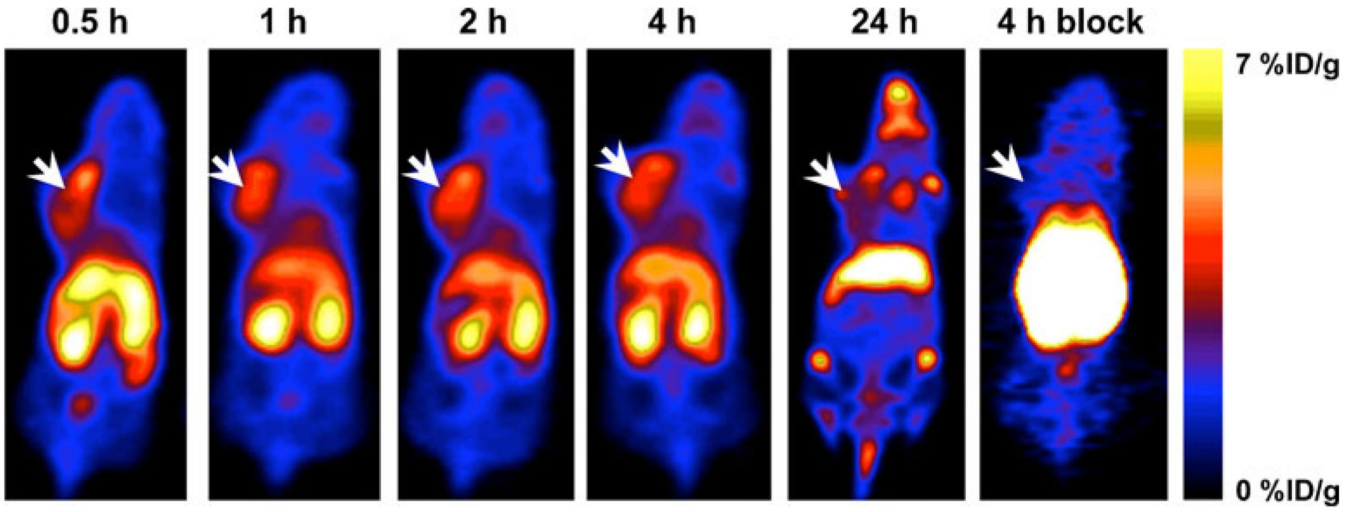

Fig. 5.

Representative PET images of an athymic nude mouse bearing orthotopic MDA-MB-435 tumor on the left mammary fat pad, at 0.5, 1, 2, 4, and 24 h post-injection of 100 μCi (3.7 MBq) of ^{89}Zr-Df-$[FK]_2$-$3PEG_4$, or co-injection with 300 μg of c(RGDfK) at 4 h post-injection. *Arrows* indicate MDA-MB-435 tumors.

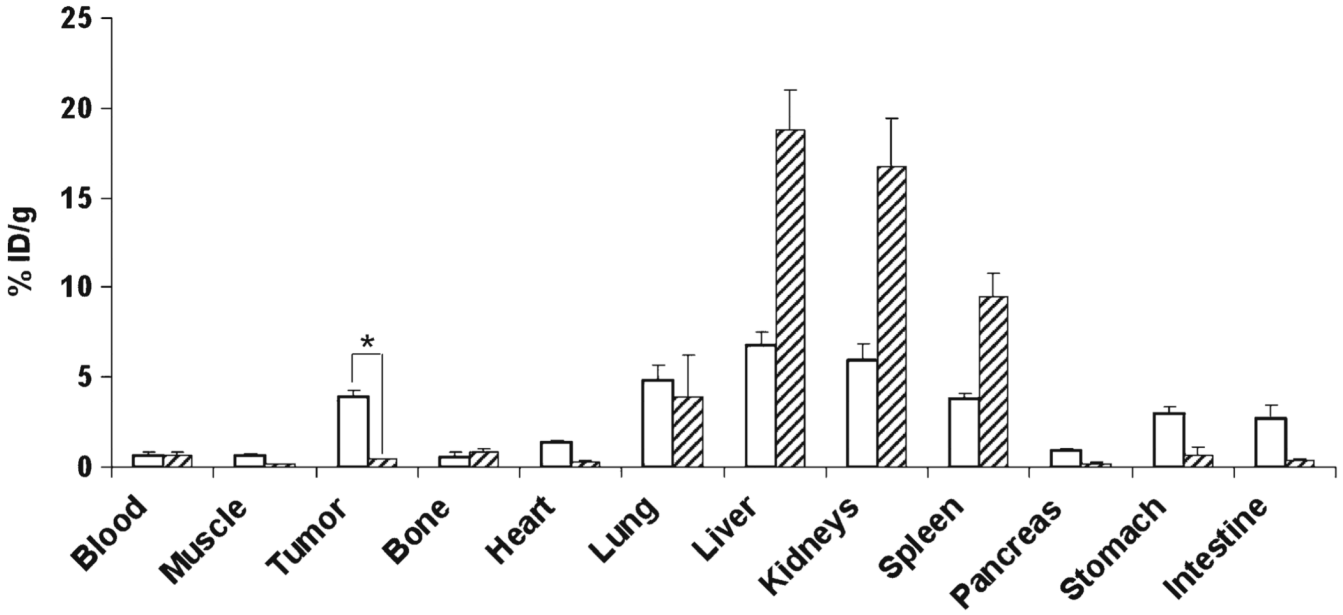

Fig. 6.

Biodistribution of MDA-MB-435 tumor-bearing mice, injected either with ^{89}Zr-Df-[FK]$_2$-3PEG$_4$ (*white bars*) or co-injection of ^{89}Zr-Df-[FK]$_2$-3PEG$_4$ with c(RGDfK) (*dash bars*) at 4 h post-injection. Results shown are averages of 4 mice±SD. *P<0.01.

Table 1

MDA-MB-435 tumor-to-blood ratios at 0.5, 1, 2, 4, and 24 h post-injection of ^{89}Zr-Df-FK, ^{89}Zr-Df-FK-PEG_3, ^{89}Zr-Df-$[FK]_2$, or ^{89}Zr-Df-$[FK]_2$-$3PEG_4$ (*n*=4 or 5 mice per group)

	^{89}Zr-Df-FK	**^{89}Zr-Df-FK-PEG_3**	**^{89}Zr-Df-$[FK]_2$**	**^{89}Zr-Df-$[FK]_2$-$3PEG_4$**
0.5 h	–	–	8.91±3.43	12.55±1.07
1 h	4.46±0.80	3.37±0.87	14.39±2.03	16.21±3.23
2 h	8.71±1.81	6.33±1.27	16.40±5.54	18.21±2.52
4 h	–	–	16.58±1.54	19.69±3.99
24 h	2.26±0.09	2.4±0.61	10.29±1.50	10.82±1.31

Table 2

Biodistribution of ^{89}Zr-Df-FK and ^{89}Zr-Df-FK-PEG$_3$ in MDA-MB-435 tumor-bearing mice at 24 h post-injection

	^{89}Zr-Df-FK	**^{89}Zr-Df-FK-PEG$_3$**
Blood	0.45±0.01	0.32±0.12
Muscle	0.23±0.01	0.19±0.01
Tumor	1.01±0.08	0.73±0.07
Bone	1.71±0.59	1.14±0.30
Heart	0.47±0.03	0.31±0.03
Lung	1.18±0.17	0.67±0.10
Liver	22.25±4.79	17.20±7.64
Kidneys	10.72±1.04	5.65±1.10
Spleen	7.19±2.13	8.94±5.89
Pancreas	0.36±0.02	0.28±0.02
Stomach	1.13±0.03	0.80±0.08
Intestine	1.14±0.20	0.71±0.07

Results shown are averages of 4–5 mice±SD

Table 3

Biodistribution of ^{89}Zr-Df-$[FK]_2$ in MDA-MB-435 tumor-bearing mice at 4 h post-injection

	^{89}Zr-Df-$[FK]_2$
Blood	0.47±0.25
Muscle	0.48±0.11
Tumor	4.04±0.73
Bone	1.66±0.44
Heart	2.01±1.86
Lung	3.49±0.56
Liver	17.46±1.85
Kidneys	21.11±3.41
Spleen	5.86±0.92
Pancreas	1.03±0.22
Stomach	2.80±0.42
Intestine	2.50±0.37

Results shown are averages of 4–5 mice±SD